RSC Advances

ROYAL SOCIETY OF CHEMISTRY

www.rsc.org/advances

Integration of Upconverting β-$NaYF_4$:Yb^{3+},Er^{3+}@TiO_2 Composites as Light Harvesting Layer in Dye-Sensitized Solar Cells

*Nathan C. Dyck, George P. Demopoulos**

$NaYF_4$:Yb^{3+},Er^{3+}@TiO_2 "core-shell" composites are integrated into DSSCs as a light harvesting layer, increasing efficiency by a factor of 1.16.

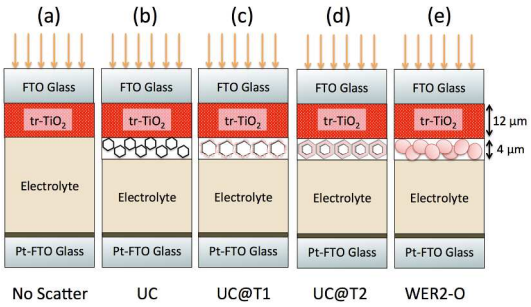

RSC Advances RSCPublishing

ARTICLE

Integration of Upconverting β-$NaYF_4$:Yb^{3+},Er^{3+}@TiO_2 Composites as Light Harvesting Layer in Dye-Sensitized Solar Cells

Cite this: DOI: 10.1039/x0xx00000x

Received 00th January 2012,
Accepted 00th January 2012

DOI: 10.1039/x0xx00000x

www.rsc.org/

N. C. Dyck[a] and G. P. Demopoulos[a]

Near infrared-to-visible upconverting $NaYF_4$:Yb^{3+},Er^{3+}@TiO_2 composites are engineered by controlled titanium dioxide coating of citrate-modified β-$NaYF_4$:Yb^{3+},Er^{3+} sub-microcrystals of ~300 nm in size and employed as light harvesting layers in dye-sensitized solar cell fabrication. The NIR-to-Vis upconversion response of the as-prepared composites is enhanced by 2 orders of magnitude increase in the upconversion luminescence as a result of annealing effects induced by the thermal processing steps involved in DSSC fabrication. In addition, the TiO_2 coating suppresses the β to α phase transition in the $NaYF_4$ thereby maximizing the upconversion response. The as-prepared upconversion crystals as well as 2 types of composite materials are integrated as internal light-harvesting layers in dye-sensitized solar cells (DSSCs). The insertion of the as-prepared or TiO_2 coated β-$NaYF_4$:Yb^{3+},Er^3 crystals with inadequate TiO_2 thickness results in a decrease in photovoltaic performance due to increased charge recombination. By ensuring the β-$NaYF_4$:Yb^{3+},Er^3 crystals are fully coated in TiO_2 ("core@shell" configuration), their integration into the DSSC is optimized, resulting in 16% relative increase in power-conversion efficiency over the control devices without the $NaYF_4$:Yb^{3+},Er^{3+}@TiO_2 composite internal layer. This increase, as determined by EIS and IPCE under 1 sun illumination, is attributed to recovery of adequate charge recombination resistance and light harvesting enhancement via scattering.

1. Introduction

As the world continues to consume non-renewable sources of fossil fuels, more and more attention is being given to renewable sources of energy such as solar power. The sun is a massive, largely untapped, energy resource. Photovoltaic devices are able to harness the power of the sun by converting the solar energy to electrical energy, however large-scale deployment is hindered by the relatively high cost of current photovoltaic technologies. The classic efficiency limit of a single junction solar cell is about 30%[1] and research level silicon cells and thin-film cells (CIGS, CdTe) have reached efficiencies as high as 25% and 20% respectively[2–4]. Dye-sensitized solar cells (DSSCs)[5–7] and other third-generation PV technologies such as organic PV[8], quantum dots[9], and perovskites[10,11] have seen an explosion in research growth in recent years due largely in part to the promise of low material and processing costs. All these research level cell technologies however have poorer energy conversion efficiencies compared to first and second-generation photovoltaic technologies.

Spectral engineering via upconversion is an approach that potentially can lead to increased efficiencies for these types of devices. Considering for example the standard dye-sensitized solar cell[7] as case study, we note that the typical light absorbing dye, a ruthenium-based complex known as N-719, has a bandgap (HOMO/LUMO gap) of ~1.6 eV. Most of the energy losses at this energy level come from sub-bandgap photons[12], making DSSCs sensitized with these types of dyes ideal candidates for upconversion. Upconversion is a process that converts two or more low energy photons into a single higher energy photon. While many upconversion mechanisms exist, energy transfer upconversion (ETU) via the Yb^{3+}-Er^{3+} lanthanide pair is the most efficient[13]. By far β-$NaYF_4$ is the most efficient host material for Yb^{3+}-Er^{3+} upconversion pair, with an optimal doping profile of 18% Yb^{3+} and 2% Er^{3+} replacing Y^{3+} in the host lattice[14]. Recent work in our laboratory has demonstrated that via crystal engineering and annealing the upconversion efficiency of β-$NaYF_4$:18%Yb^{3+},2%Er^{3+} can be enhanced as much as three orders of magnitude[15,16]. Infrared-to-visible upconversion has attracted a great deal of attention with potential applications as biological markers[17–19], photonic devices[20–22], and solar cells[12,23–38].

Recently, application of these materials as internal layers in DSSCs has been the subject of a number of studies[23,27–29,32,30,18,31,33]. Shan and Demopoulos investigated the effect of an internal LaF_3:Yb^{3+},Er^{3+}-TiO_2 layer and demonstrated proof-of-concept NIR operation but ultimately saw drops in performance associated with charge recombination[23]. Another study by Wang *et al.* used YOF:Yb^{3+},Er^{3+} upconversion materials in the TiO_2 photoanode layer to increase overall conversion efficiency by a factor of 1.23[32]. More recently, Zhang *et al.* fully replaced the TiO_2 photoanode material with a $NaYF_4$:Yb^{3+},Er^{3+}@TiO_2 core-shell composite material,

attaining enhancement of the conversion efficiency by a factor of 1.23[33]. Similarly, Liang *et al.* used double-shell β-$NaYF_4$:Yb^{3+},Er^{3+}/SiO_2/TiO_2 submicroplates and obtained 29.4% improvement in efficiency[28]. In all these studies, however, insufficient effort has been placed on optimizing and understanding the best way to integrate the UC materials, and more importantly in analysing and quantifying the relative contributions of upconversion and internal light scattering in device's improved PV performance.

In the present study, β-$NaYF_4$:Yb^{3+},Er^{3+} sub-microcrystals were prepared using a citrate-stabilized hydrothermal approach to control particle size and morphology. These sub-microcrystals were coated with TiO_2 ("core@shell" configuration type) to aid with integration into DSSCs as a scattering layer in such way that prevents charge recombination losses. The upconversion properties of the composite material are investigated, with attention given to the effect of the DSSC thermal processing steps and the true magnitude of upconversion contribution to light harvesting enhancement in the solar cell devices. The cells prepared were tested using a host of photovoltaic and electrochemical testing procedures, including performance under simulated solar illumination as well as NIR laser illumination.

2. Experimental

2.1 $NaYF_4$:Yb^{3+},Er^{3+} Synthesis

$NaYF_4$:18%Yb^{3+},2%Er^{3+} was produced by a citrate modified hydrothermal method, with a target particle size of 300 nm based on previous work in our lab[15]. Sodium citrate (54 mmol) was first dissolved into 40 mL of deionized water. Following this, $Y(NO_3)_3 \cdot 6H_2O$ (1.6 mmol), $Yb(NO_3)_3 \cdot 5H_2O$ (0.36 mmol), and $Er(NO_3)_3 \cdot 5H_2O$ (0.04 mmol) was added to the solution and stirred until dissolved. Finally, an amount of NaF (18 mmol) was added to the solution and stirred for 15 minutes. The solution was transferred to a 125 mL stainless steel pressure vessel (Parr Instruments) with Teflon liner and heated hydrothermally at 200°C for 2 hours, producing β-hexagonal phase particles of about 300 nm in size (Figure S3, ESI). After hydrothermal treatment, the resulting precipitate was separated by centrifugation and then washed 3 times with deionized water and once with ethanol. The resulting solids were dried at 80 °C for 24 hours.

2.2 UC@TiO_2 Composite Synthesis

For production of the composite upconverter material a modified process was adopted from Zhang *et al.*[39]. Amorphous titanium dioxide was deposited on the surface of suspended particles in solution based on hydrolysis of titanium ethoxide in ethanol followed by condensation of titanium dioxide. Typically 0.03 g of the $NaYF_4$:Yb^{3+},Er^{3+} sub-microcrystals produced were taken and dispersed in 30 mL of anhydrous ethanol using an ultrasonic horn. Following this, 3 mmol of titanium ethoxide (TEOT) was added to the suspension under vigorous stirring. A separate solution was prepared with 30 mL of anhydrous ethanol and an amount of deionized water (DIW, 9 mmol or 18 mmol), which was then added drop wise to the first solution to give an overall DIW:TEOT molar ratio of 3:1 or 6:1 depending on sample. The resulting solution was stirred with a magnetic stir bar, at room temperature, for 2 hours, after which the solids were separated by centrifugation (6000 RPM, 5 min) and washed twice with anhydrous ethanol. The resulting solids were dried at 80 °C for 24 hours.

2.3 Dye-Sensitized Solar Cell Fabrication

DSSC photoanodes were prepared using screen-printing. Transparent FTO glass was washed ultrasonically in an aqueous detergent solution (Micro 90) for 15 minutes and rinsed with water and ethanol. Two layers of transparent TiO_2 (18NR-T, Dyesol) were screen printed (AT-25PA, ATMA), drying the layers for 15 minutes at 80 °C between print runs (typically 6 μm/run), giving a total transparent layer thickness of 12 μm. Depending on the cell type, an additional scattering layer of 4 μm was screen printed, using either an industrial benchmark paste (WER2-O, Dyesol) or using pastes prepared with the as-is $NaYF_4$:Yb^{3+},Er^{3+} crystals or the $NaYF_4$:Yb^{3+},Er^{3+}@TiO_2 composite particles. The procedure used for preparing pastes is published elsewhere[40,41]. The photoanode was annealed at 450 °C for 30 minutes according to a heating profile (Figure S1, ESI). The photoanode was then submerged in a 40 mM $TiCl_4$ aqueous solution at 80 °C for 30 minutes, and annealed a second time at 450 °C for 30 minutes. In the case of cells prepared using the $NaYF_4$:Yb^{3+},Er^{3+} and the $NaYF_4$:Yb^{3+},Er^{3+}@TiO_2 (DIW:TEOT, 3:1) scattering pastes, the $TiCl_4$ treatment removes the scattering layer by dissolving it. As such, in these cells the scattering layer was printed after the $TiCl_4$ treatment and second annealing in order to avoid removal by the $TiCl_4$ treatment. These cells were annealed a 3rd time using the same profile.

The photoanode was then sensitized using a 0.5 M N-719 dye solution in ethanol for 24 hours. In the case of cells prepared using the $NaYF_4$:Yb^{3+},Er^{3+} and $NaYF_4$:Yb^{3+},Er^{3+}@TiO_2 (DIW:TEOT, 3:1) scattering pastes, a longer sensitization time of 72 hours was needed. A platinized counter-electrode was produced using pre-drilled FTO glass cleaned in a similar fashion to the photoanode. A drop (~8 μL) of H_2PtCl_6 (50 mM in isopropanol) was spread across the surface of the counter electrode and annealed at 400 °C for 30 minutes.

The cells were then sealed in a sandwich type configuration using a hot melt ionomer film (Surlyn, 30 μm) using a cell assembly machine (E002-1233, Dyesol). The cells were injected with an I_3^-/I^- liquid electrolyte (EL-HPE, Dyesol) through the pre-drilled holes, filling via capillary forces. The holes were sealed using a coverslip and the hot melt ioner film. Details relating to cell characterization can be found in the ESI.

3. Results and Discussion

3.1. Upconversion Composites

Hexagonal β-phase $NaYF_4$:Yb^{3+},Er^{3+} crystals (~300 nm in size) were produced by a citrate modified hydrothermal process [15]. These crystals were then incorporated into a core-shell type composite material with TiO_2 via directed hydrolysis of titanium ethoxide in ethanol. The water hydrolyzes the titanium ethoxide after which a condensation reaction occurs, depositing amorphous TiO_2 onto the upconverter particle surfaces, according to the following reactions (R = C_2H_5)[42];

$$Ti(OR)_4 + 3H_2O \rightarrow Ti(OR)(OH)_3 + 3ROH$$

and

$$Ti(OR)(OH)_3 \rightarrow TiO_2 \cdot xH_2O + (1-x)H_2O + ROH$$

The rate of reaction and therefore the amount of TiO_2 deposited as a shell depends on the molar ratio of DIW:TEOT and therefore the extent of the hydrolysis reaction. TEM images are presented in Figure 1, showing the difference between the 3:1 DIW:TEOT ratio (UC@T1) and the 6:1 DIW:TEOT ratio (UC@T2) materials.

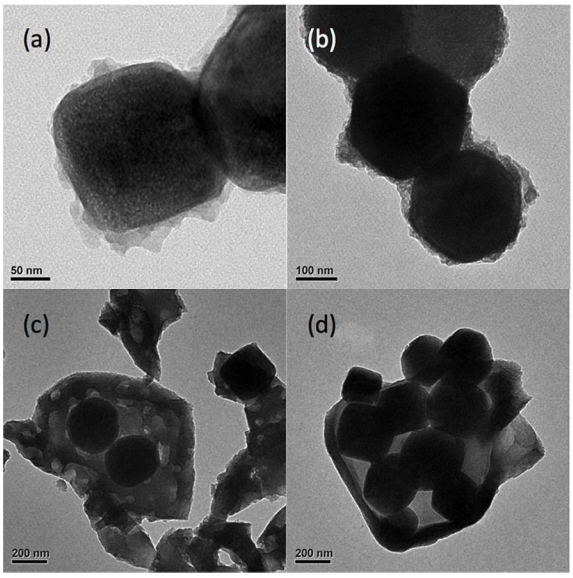

Figure 1. TEM images of the UC@TiO_2 composite materials showing UC@T1 particles produced with 3:1 DIW:TEOT ratio (a,b), and UC@T2 particles produced with 6:1 DIW:TEOT ratio (c,d)

As can be seen, the particles in UC@T1 are covered by an incomplete shell of amorphous TiO_2, while the particles in UC@T2 are either completely covered by a thicker amorphous TiO_2 shell or embedded into a larger amorphous TiO_2 matrix on the order of ~1 μm.

$NaYF_4$:Yb^{3+},Er^{3+} upconversion materials convert infrared light to both red and green visible light. Both the shape and intensity of the upconversion spectrum is important for proper technological application. The phase of the UC material is also very important in determining both these aspects. The β-hexagonal phase of $NaYF_4$ is a much better upconverter compared with its α-cubic counterpart[14]. In addition, the β-phase emits predominantly green light while the α-phase emits predominantly red. This is an important aspect when engineering these materials for DSSCs as the dye absorbs green light more strongly than red and as a result, the DSSC performs better under green illumination[43,23]. Since the red and green upconversion processes compete for upconverted energy, it is important to ensure that the amount of α-phase is minimized in order to maximize the coupling of the upconverted light to the solar cell through green upconversion. The upconversion fluorescence spectra of the as-prepared UC sub-microcrystals and the composite UC materials are shown in Figure 2(a).

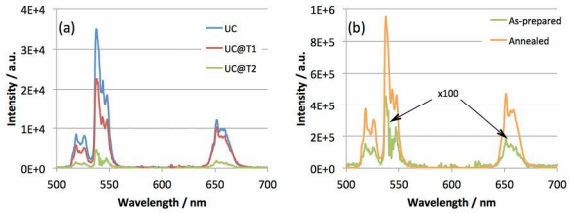

Figure 2. Upconversion fluorescence spectra under 980 nm NIR laser illumination showing (a) the difference between the as-prepared UC and the UC@TiO_2 materials, and (b) the difference between the as-prepared UC@T2 material (spectrum multiplied by 100 for easier visual comparison) and the annealed UC@T2 material

The efficiency of the upconversion process in bulk $NaYF_4$:Yb^{3+},Er^{3+} is modest, and decreases further when the particle size of the crystals is smaller than a few microns [13]. Other studies have increased the upconversion fluorescence intensity by using a core-shell approach to eliminate non-radiative pathways by separating the upconverting core from the quenching surface states[44,45]. In the current study, a decrease is observed in Figure 2(a) with addition of a TiO_2 shell in the composite materials. UC@T1 has about 2/3 the upconversion intensity of the as-prepared UC material, while UC@T2 only has about 1/10 the upconversion intensity. This decrease is largely attributed to the decreasing absolute mass of UC crystals being excited due to the lower fraction of UC material in the composite powder as a whole. While it is possible to decouple these effects to see how the presence of the TiO_2 affects upconversion in an equivalent number of excited crystals, in the context of solar cell integration, especially that of internal DSSC application, there are limitations placed on the amount of material that can be used within the cell itself based on the volume of the internal chamber, meaning that the primary concern should be the upconversion of an equivalent volume of scattering material rather than volume of upconverting material. Therefore examining the upconversion fluorescence of the composite powder as a whole is justified.

Another important consideration with regards to upconversion is the presence of organic molecules on the surface of the upconversion particles. The as-prepared particles were modified with citrate in order to control both the particle shape and size[15,16]. The presence of organic molecules on the surface of upconversion particles has been shown to quench the upconversion fluorescence due to high-energy vibrational modes[46], and is something that should be avoided for solar cell

integration. Annealing is a very effective way to increase the upconversion fluorescence of citrate-modified UC particles both through removal of organics as well as removal of internal defects in the crystal lattice that otherwise quench the upconverted energy states[46,16]. In the case of the DSSCs assembled in this study, a standard DSSC annealing process (at 450 °C) was used to sinter the TiO_2 sub-microcrystalline layer and remove the organic additives from the pastes used for screen-printing (Figure S1, ESI). Very advantageously, the same sintering process also serves to anneal the printed upconversion scattering layer, resulting in an impressive increase of the upconversion fluorescence of the UC@T2 material by over 2 orders of magnitude as can be seen in Figure 2(b).

Although annealing clearly increases the upconversion fluorescence in the material, it can also cause partial transformation from the β-phase to the α-phase at temperatures as low as 400 °C[15]. In order to investigate possible phase transformations, XRD was performed on the as-prepared and annealed UC and UC@T2 materials, as shown in Figure 3.

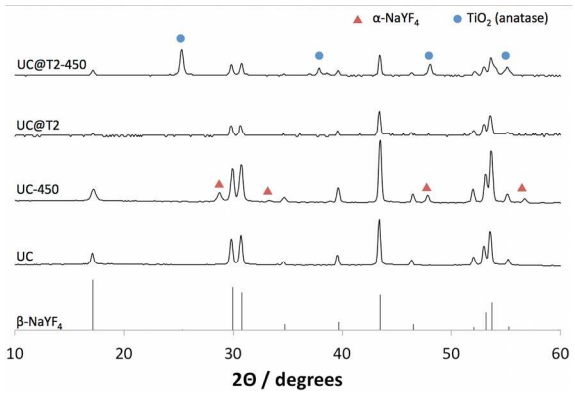

Figure 3. Powder XRD results showing the effect of annealing at 450 °C on the uncoated UC material and the UC@TiO_2 material. Reference pattern for β-$NaYF_4$ (JCPDS 28-1192) is included and peaks corresponding to α-$NaYF_4$ and TiO_2 (anatase phase) are indicated with markers

From the XRD traces it can be seen that both UC and UC@T2 as-prepared materials are pure β-$NaYF_4$. When sample UC is annealed at 450 °C, a partial transformation to α-phase is observed as indicated in Figure 3, however for the UC@T2 material, we see that the phase transition is suppressed, possibly because the formation of crystalline TiO_2 is more kinetically favoured and energy is initially directed towards the TiO_2 material transformation. This preserves the β-phase $NaYF_4$ of the core particles and helps to maintain a high green-to-red ratio[14]. From the XRD results we also see appearance of crystalline TiO_2 peaks (anatase) in the annealed UC@T2 material, indicating that the amorphous shell is converted to crystalline TiO_2. TiO_2 has a number of polymorphs, although anatase has been shown to have the best performance in DSSC devices due to its preferable bandgap and conduction band edge[47], and its presence is important for internal application of upconverter materials[33]. In summary, the annealing process serves as a multifunctional tool, sintering the sub-microtitania-based photoanode, increasing the upconversion fluorescence, and converting the amorphous TiO_2 to anatase, while the presence of the TiO_2 shell helps to suppress the β-to-α phase transformation, maintaining a high green-to-red ratio.

3.2. Dye-Sensitized Solar Cell Integration

The upconvertor materials were incorporated into pastes and screen-printed as scattering layers in DSSC devices. In addition to the 3 types of upconversion materials investigated, 2 types of control devices were also fabricated, one type without a scatter layer, and another using a commercially available scatter paste comprised of ~200 nm anatase sub-microparticles. All device types investigated are shown schematically in Figure 4. For each type of scatter layer, multiple cells were made and tested under 1 sun illumination. The results are tabulated in Table 1, with the current-voltage relationships of selected devices from each series presented in Figure 5.

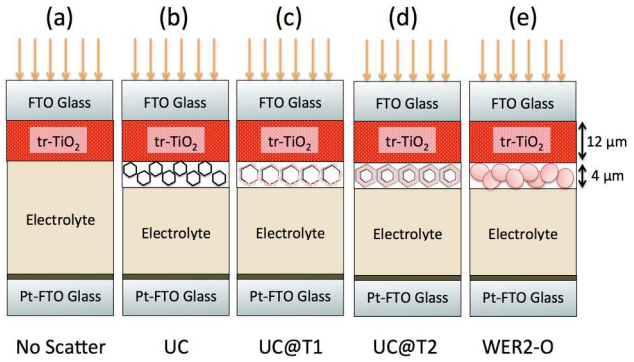

Figure 4. Schematic representation of the DSSC devices. Part (a) shows the device without scatter layer, (b) shows the device using the UC material, (c) shows the device using the UC@T1 material with incomplete TiO_2 coating, (d) shows the device using the UC@T2 material with complete TiO_2 coating, and (e) shows the device using the commercial WER2-O TiO2 scatter layer.

Table 1. Detailed PV characteristics for different UC/scattering layers studied. All values are an average of multiple cells made under the same conditions, with the standard deviation of each device set listed as the error on each value.

Scatter Layer	Thickness (μm) tr[a)]	Thickness (μm) sc[b)]	J_{sc} (mA/cm^2)	V_{oc} (V)	FF	η (%)	Dye Loading (10^{-7} mol/cm^2)
None	12	--	12.6 ± 0.6	0.7 ± 0.02	0.71 ± 0.03	6.21 ± 0.5	1.64
UC	12	4	4.1 ± 0.4	0.76 ± 0.01	0.79 ± 0.01	2.48 ± 0.2	1.50
UC@T1	12	4	4.4 ± 0.5	0.76 ± 0.02	0.76 ± 0.05	2.5 ± 0.2	1.36
UC@T2	12	4	13.4 ± 0.2	0.73 ± 0.005	0.74 ± 0.01	7.22 ± 0.1	1.75
WER2-O	12	4	14.6 ± 0.1	0.72 ± 0.01	0.73 ± 0.01	7.73 ± 0.1	1.70

[a)]transparent; [b)] scattering

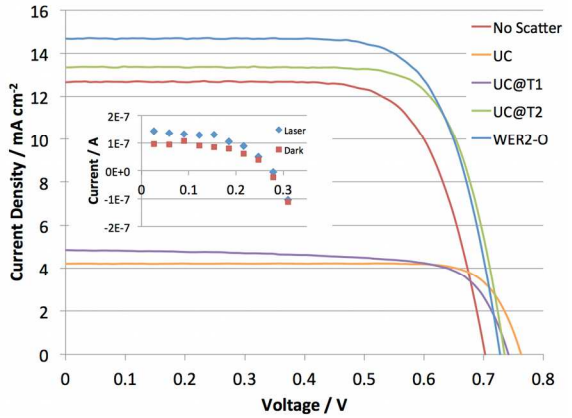

Figure 5. Current-voltage characteristics for different UC/scattering layers investigated. Inset: current voltage relationship for UC@TiO2 device under 980 nm laser illumination, illustrating proof-of-concept IR function.

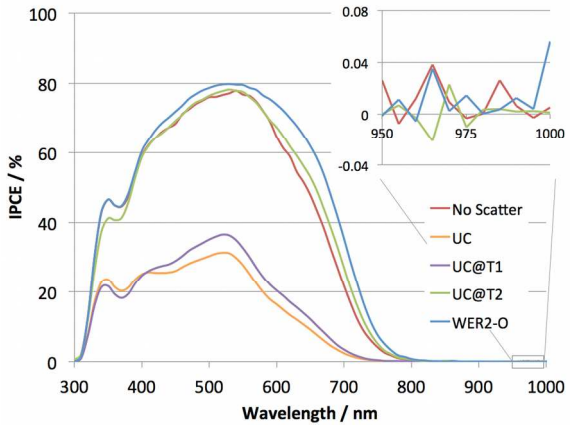

Figure 6. Incident photon to electron conversion (IPCE) for different UC/scattering layers studied. All measurements were performed under ~1 sun light bias. Inset: detailed view of device performance in the NIR region.

The transparent control device without a scatter layer has an efficiency (η) of 6.21%, and it is immediately apparent that both the UC and UC@T1 scatter layers result in a severe drop in efficiency to 2.48% and 2.5%, respectively. This difference is due to a drop in the J_{sc} of the devices from 12.6 mA/cm^2 in the control to 4.1 and 4.4 mA/cm^2 in the UC and UC@T1 devices, respectively. Part of this drop can be attributed to a lower dye loading in the UC and UC@T1 devices, as can be seen in Table 1. Both the UC and UC@T1 devices required longer sensitization times, and despite this, the dye loading is still not as high as in the control devices, possibly because the additional layers hinder diffusion of the dye into the porous TiO_2 layer. It is clear that the presence of these layers interferes with the sensitization process, and contributes to the decrease in the J_{sc}. On the other hand, the UC@T2 devices show efficiencies of 7.22%, a 16% relative increase in efficiency over the transparent control device without scatter layer. This increase comes from both a higher J_{sc} and V_{oc}, both of which are characteristic of scattering layers. NIR performance of the device is demonstrated as proof-of-concept with 980 nm laser illumination and is shown in the inset of Figure 5. The difference between the dark current and the current under illumination is small, however this can be partially attributed to the very small spot size of the laser. Although an increase in performance is seen in the UC@T2 devices, it does not match the performance of the commercially available scattering layer, WER2-O, which gave the highest efficiencies observed in this study at 7.73%.

To further investigate the effect of the UC@TiO_2 scattering layers, the incident photon-electron conversion efficiency (IPCE) was measured, giving the spectral response of the cells. These results are shown in Figure 6.

From the plot, it can be seen that the UC and UC@T1 devices have a much lower IPCE than that of the transparent control. The UC@T1 device has a slightly higher IPCE than the UC device, which is attributed to stronger scattering in the UC@T1 device. This was observed visually as a higher degree of transparency observed in the UC scatter layer devices (Figure S2, ESI). The refractive indices of the DSSC electrolyte, $NaYF_4$, and TiO_2 are about 1.4, 1.5, and 2.0, respectively. Since scattering relies on large changes in the material refractive index, TiO_2 is a much more effective scattering agent than $NaYF_4$ and the coated UC@T1 particles scatter more light than the uncoated UC particles.

UC@T2 provides higher IPCE response than the control device without scatter layer in the visible range and even extending slightly into the NIR from 300 nm to 800 nm. The IPCE of the commercial paste shows the highest response.

It is very important to note that the IPCE spectrum shows essentially no response near the absorption range of the Yb^{3+} ion as shown in the inset of Figure 6. If a response is present, it does not exceed the noise of the measurement, corresponding to ±0.05%. Even if the contributions of upconversion were equivalent to the noise level, it would be negligibly small compared to the benefit coming from scattering. It should be noted that there was also no observable NIR response from the UC and UC@T1 devices (results not shown).

The efficiency, η_{UC}, of an n-photon upconversion process is as follows[48],

$$\eta_{UC} \propto irradiance^{n-1} \quad (1)$$

Where n is the number of photons required for a single upconverted photon (in this case, $n \approx 2$). The irradiance power density is therefore very important for evaluating the upconversion performance. The IPCE measurements were carried out using a bias light to roughly simulate 1 sun illumination. Even under the maximum bias light voltage (corresponding only to about 2.5 sun), a measureable response (>0.05%) in the 950-1000 nm region was unattainable. It is

possible that higher solar concentration may be able to increase the upconversion contribution, as has been seen experimentally in amorphous silicon solar cell devices[34] as well as in theoretical calculations in a similar $NaYF_4:Er^{3+}$ upconversion system[12]; however light concentration can cause elevated temperatures in DSSCs, which can cause subsequent problems with other areas of DSSC functioning if not properly handled[49]. While NIR laser illumination can been used to show proof-of-concept upconversion coupling in other studies[33,27,28] as well as in the current study, its use should be avoided unless the technological application warrants the power densities used. In the case of photovoltaic application, in the absence of light concentration, this is clearly not the case. Other studies have additionally used an IR-pass filter for demonstration of NIR DSSC performance[32,27] however this type of measurement is often unable to decouple the scattering effect from the upconversion if the cut-off wavelength of the filter is not selected properly. IPCE measurements under anticipated illumination provide the best assessment of the true contribution from upconversion. As has been seen from the results presented here, that contribution is negligible.

3.2.1. Electrochemical Impedance Spectroscopy (EIS)

In order to further understand the impact of the UC scattering layers on the internal functioning of the DSSC, a technique known as electrochemical impedance spectroscopy (EIS) was employed. EIS is a very versatile technique that reveals information about electronic and ionic kinetics at work in the solar cell.

In order to extract the various operational parameters of the solar cell, an equivalent circuit originally developed by Fabregat-Santiago *et al.*[50,51], was used to fit the impedance data. The model, shown in Figure 7 includes a number of useful performance parameters including the series resistance of the solar cell, R_s, the transport resistance, r_{tr}, the chemical capacitance, c_μ, and the charge transfer resistance from the TiO_2 to the electrolyte, r_{CT}. For the fitting, all capacitors were treated as constant phase elements.

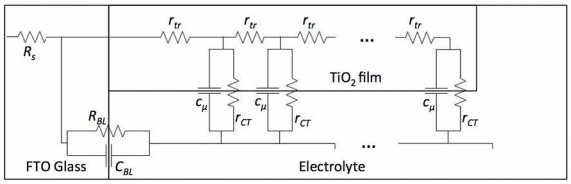

Figure 7. Equivalent circuit used for extraction of solar cell performance parameters, originally developed by Fabregat-Santiago *et al.* [49,50]

The chemical capacitance of the film, C_μ (= $c_\mu L$) is plotted in Figure 8(a) against the Fermi voltage (V_F) of the film. V_F is proportional to the Fermi level of the electrons in the sub-microcrystalline TiO_2 and is calculated by removing the voltage drop due to series resistance (R_s) in the solar cell by using the following equation[50]:

$$V_F = V_{app} - V_S = V_{app} + jR_S \qquad (2)$$

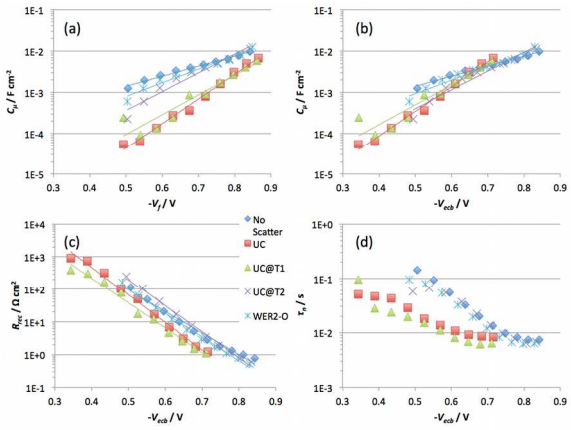

Figure 8. Electrochemical impedance spectroscopy (EIS) of different UC/scattering layers investigated under 1 sun illumination, showing (a) chemical capacitance, C_μ, plotted against V_F, (b) chemical capacitance, C_μ, plotted against V_{ecb}, (c) recombination resistance, R_{rec}, plotted against V_{ecb}, and (d) carrier lifetime, τ_n, plotted against V_{ecb}.

The primary pathway for loss of excited carriers is via electron recombination from the conduction band of the TiO_2 to the electrolyte, which is dictated by the recombination resistance, R_{rec} (= r_{CT}/L). The recombination resistance is proportional to the position of the TiO_2 conduction band, which can be displaced through the use of different dyes, electrolytes, and pastes[50]. As such, a voltage shift, ΔE_C, must be introduced, with R_{rec} being plotted against an "equivalent conduction band" potential, $V_{ecb} = V_F - \Delta E_C / q$.

This is accomplished by shifting the C_μ plot so that all curves overlap in relation to a reference sample (in this case, the control without scatting layer), as is seen in Figure 8(b).

R_{rec} can now be plotted vs. V_{ecb} as shown in Figure 8(c). The recombination resistance is similar in the control device without scattering layer, the UC2@T2, and the WER2-O devices, while it is lower in the UC and UC@T1 devices indicating increased recombination rates. These increased recombination rates are the primary reason for the J_{sc} decreases seen in the UC and UC@T1 devices (see Figure 5 and Table 1). Similarly, the electron lifetime can be calculated using the equation, $\tau_n = R_{rec}C_\mu$ and is plotted in Figure 8(d), showing lower electron lifetimes in the UC and UC@T1 devices. These results agree with other similar studies that have suggested the presence of internal $NaYF_4$ upconversion particles contributes to electron recombination and therefore a reduction in overall device efficiency[28]. The UC device has the lowest efficiency (2.48%), which only marginally increases with the UC@T1 device (2.5%). Both the UC and UC@T1 devices have poor recombination resistance, and the UC@T1 device actually has lower electron lifetimes, so the marginal increase in efficiency must be primarily attributed to the difference coming from scattering as already discussed. It is only in the UC@T2 devices, when the UC particles are fully coated/embedded into TiO_2, that the recombination resistance and electron lifetime of the control device is recovered.

4. Conclusions

Citrate-modified $NaYF_4$:Yb^{3+},Er^{3+} NIR-to-visible upconversion sub-microcrystals as well as $NaYF_4$:Yb^{3+},Er^{3+}@TiO_2 composite materials have been integrated into DSSC devices as internal light harvesting layers. The upconversion effect of the materials has been demonstrated. The upconversion fluorescence of the TiO_2 coated UC@T2 composite material was 10 times lower than its uncoated sub-microcrystals counterpart, which was attributed to lower upconverting material mass in an equivalent volume. This drop in fluorescence was more than compensated for when the material is subjected to an annealing profile used in DSSC sintering, with over 2 orders of magnitude increase in the upconversion fluorescence.

Integration of the as-prepared UC sub-microcrystals as an internal layer causes a dramatic decrease in efficiency that is attributed to an increase in electron recombination from the TiO_2 to the electrolyte caused by the presence of the $NaYF_4$ upconversion crystals. Coating the upconversion particles with a layer of TiO_2 ("core-shell" configuration) helps to eliminate the charge recombination as well as resulting in an overall efficiency of 7.22%, a relative increase of 16% over a control device without a UC@TiO_2 internal layer (6.21%). This increase is attributed entirely to scattering, with no measurable IPCE response (>0.05%) in the 950-1000 nm region, where upconversion via the Yb^{3+}-Er^{3+} couple should, in principle, be occurring. Having demonstrated the importance of core-shell sub-microstructuring for integrating upconversion crystals in hybrid solar cells, future efforts should be geared towards the deployment of UC material blends for wider and more efficient NIR light harvesting. Similarly, UC@TiO_2 core-shell sub-microcrystals can be evaluated in combination with quantum-dot semiconducting or plasmonic metal light harvesting centres.

Acknowledgements

This work was funded by NSERC through a strategic project grant and sponsored by Targray Technology International, Versatilis, CIS Solar, and Hydro-Quebec's IREQ. N. Dyck is also the recipient of an Alexander Graham Bell CGS Scholarship from NSERC.

Notes and References

[a] Materials Engineering, McGill University, 3610 University Street, H3A 0C5, Montreal, QC, Canada

Electronic Supplementary Information (ESI) available: [details of any supplementary information available should be included here]. See DOI: 10.1039/b000000x/

1. W. Shockley and H. J. Queisser, *J. Appl. Phys.*, 1961, **32**, 510.
2. J. Zhao, A. Wang, M. A. Green, and F. Ferrazza, *Appl. Phys. Lett.*, 1998, **73**, 1991.
3. Best Research-Cell Efficiencies, NREL http://www.nrel.gov/ncpv/images/efficiency_chart.jpg, (accessed May 2014).
4. M. Green, K. Emery, Y. Hishikawa, W. Warta, and E. D. Dunlop, *Prog. Photovoltaics Res. Appl.*, 2014, **22**, 1–9.
5. B. O'Regan and M. Grätzel, *Nature*, 1991, **353**, 737–740.
6. A. Yella, H.-W. Lee, H. N. Tsao, C. Yi, A. K. Chandiran, M. K. Nazeeruddin, E. W.-G. Diau, C.-Y. Yeh, S. M. Zakeeruddin, and M. Gratzel, *Science*, 2011, **334**, 629–634.
7. H. M. Upadhyaya, S. Senthilarasu, M.-H. Hsu, and D. K. Kumar, *Sol. Energy Mater. Sol. Cells*, 2013, **119**, 291–295.
8. R. F. Service, *Science*, 2011, **332**, 293.
9. A. H. Ip, S. M. Thon, S. Hoogland, O. Voznyy, D. Zhitomirsky, R. Debnath, L. Levina, L. R. Rollny, G. H. Carey, A. Fischer, K. W. Kemp, I. J. Kramer, Z. Ning, A. J. Labelle, K. W. Chou, A. Amassian, and E. H. Sargent, *Nat. technol.*, 2012, **7**, 577–82.
10. K. Wojciechowski, M. Saliba, T. Leijtens, A. Abate, and H. J. Snaith, *Energy Environ. Sci.*, 2014, **7**, 1142.
11. S. Kazim, M. K. Nazeeruddin, M. Grätzel, and S. Ahmad, *Angew. Chem. Int. Ed. Engl.*, 2014, **53**, 2812–24.
12. A. Shalav, B. S. Richards, and M. A. Green, *Sol. Energy Mater. Sol. Cells*, 2007, **91**, 829–842.
13. F. Auzel, *Chem. Rev.*, 2004, **104**, 139–173.
14. K. Kramer, D. Biner, G. Frei, and H. Gudel, *Chem. Mater.*, 2004, **16**, 1244–1251.
15. H. Assaaoudi, G.-B. Shan, N. Dyck, and G. P. Demopoulos, *CrystEngComm*, 2013, **15**, 4739–4746.
16. N. C. Dyck, F. C. J. M. van Veggel, and G. P. Demopoulos, *ACS Appl. Mater. Interfaces*, 2013, **5**, 11661–11667.
17. G. Yi, H. Lu, S. Zhao, Y. Ge, W. Yang, D. Chen, and L.-H. Guo, *Nano Lett.*, 2004, **4**, 2191–2196.
18. Z. Chen, L. Zhang, Y. Sun, J. Hu, and D. Wang, *Adv. Funct. Mater.*, 2009, **19**, 3815–3820.
19. X. Yu, M. Li, M. Xie, L. Chen, Y. Li, and Q. Wang, *Nano Res.*, 2010, **3**, 51–60.
20. E. Downing, L. Hesselink, J. Ralston, and R. Macfarlane, *Science*, 1996, **273**, 1185–1189.
21. F. F. Zhang, Y. Wan, T. Yu, Y. Shi, S. Xie, Y. Li, L. Xu, B. Tu, and D. Zhao, *Angew. Chemie*, 2007, **119**, 8122–8125.
22. R. A. McFarlane, *Opt. Lett.*, 1991, **16**, 1397–1399.
23. G.-B. Shan and G. P. Demopoulos, *Adv. Mater.*, 2010, **22**, 4373–7.
24. J. de Wild, A. Meijerink, J. K. Rath, W. G. J. H. M. van Sark, and R. E. I. Schropp, *Energy Environ. Sci.*, 2011, **4**, 4835–4848.
25. G.-B. Shan, H. Assaaoudi, and G. P. Demopoulos, *ACS Appl. Mater. Interfaces*, 2011, **3**, 3239–3243.
26. Y. Y. Cheng, B. Fückel, R. W. MacQueen, T. Khoury, R. G. C. R. Clady, T. F. Schulze, N. J. Ekins-Daukes, M. J. Crossley, B. Stannowski, K. Lips, and T. W. Schmidt, *Energy Environ. Sci.*, 2012, **5**, 6953–6959.
27. Y. Li, K. Pan, G. Wang, B. Jiang, C. Tian, W. Zhou, Y. Qu, S. Liu, L. Feng, and H. Fu, *Dalt. Trans.*, 2013, **42**, 7971–9.
28. L. Liang, Y. Liu, and X.-Z. Zhao, *Chem. Commun.*, 2013, **49**, 3958–60.
29. Y. Li, G. Wang, K. Pan, B. Jiang, C. Tian, W. Zhou, and H. Fu, *J. Mater. Chem.*, 2012, **22**, 20381.
30. C. Yuan, G. Chen, P. N. Prasad, T. Y. Ohulchanskyy, Z. Ning, H. Tian, L. Sun, and H. Ågren, *J. Mater. Chem.*, 2012, **22**, 16709.
31. C. Han, H. Lee, and K. Lee, *Bull. Korean Chem. Soc.*, 2009, **30**, 219–223.

32. J. Wang, J. Lin, J. Wu, M. Huang, Z. Lan, Y. Chen, S. Tang, L. Fan, and Y. Huang, *Electrochim. Acta*, 2012, **70**, 131–135.
33. J. Zhang, H. Shen, W. Guo, S. Wang, C. Zhu, F. Xue, J. Hou, H. Su, and Z. Yuan, *J. Power Sources*, 2013, **226**, 47–53.
34. J. de Wild, T. F. Duindam, J. K. Rath, A. Meijerink, W. G. J. H. M. van Sark, and R. E. I. Schropp, *IEEE J. Photovoltaics*, 2013, **3**, 17–21.
35. X. Wu, G. Q. Max Lu, and L. Wang, *Adv. Energy Mater.*, 2013, **3**, 704–707.
36. A. Nattestad, Y. Cheng, R. W. MacQueen, T. F. Schulze, F. Thompson, A. Mozer, B. Fuckel, T. Khoury, M. Crosslet, K. Lips, G. Wallace, and T. W. Schmidt, *J. Phys. Chem. Lett.*, 2013, **4**, 2073–2078.
37. W. Zou, C. Visser, J. a. Maduro, M. S. Pshenichnikov, and J. C. Hummelen, *Nat. Photonics*, 2012, **6**, 560–564.
38. Y. Y. Cheng, B. Fückel, R. W. MacQueen, T. Khoury, R. G. C. R. Clady, T. F. Schulze, N. J. Ekins-Daukes, M. J. Crossley, B. Stannowski, K. Lips, and T. W. Schmidt, *Energy Environ. Sci.*, 2012, **5**, 6953.
39. D. Zhang, D. Zhao, K. Zheng, N. Liu, and W. Qin, *J. Nanosci. Nanotechnol.*, 2011, **11**, 9761–9764.
40. C. Charbonneau, R. Gauvin, and G. P. Demopoulos, *J. Electrochem. Soc.*, 2011, **158**, H224.
41. S. Ito and P. Chen, *Prog. Photovoltaics Res. Appl.*, 2007, **15**, 603–612.
42. E. Barringer and H. Bowen, *Langmuir*, 1985, **1**, 414–420.
43. K. Fantai, D. Songyuan, and W. Kongjia, *Plasma Sci. Technol.*, 2006, **8**, 3–7.
44. H. Mai and Y. Zhang, *J. Phys. Chem. C*, 2007, **111**, 13721–13729.
45. G. Yi and G. Chow, *Chem. Mater.*, 2007, **19**, 341–343.
46. Y. Wang, L. Tu, J. Zhao, and Y. Sun, *J. Phys. Chem. C*, 2009, **113**, 7164–7169.
47. A. Hagfeldt, G. Boschloo, L. Sun, L. Kloo, and H. Pettersson, *Chem. Rev.*, 2010, **110**, 6595–663.
48. M. Pollnau and D. Gamelin, *Phys. Rev. B*, **61**, 2000.
49. N. Jiang, T. Sumitomo, T. Lee, A. Pellaroque, O. Bellon, D. Milliken, and H. Desilvestro, *Sol. Energy Mater. Sol. Cells*, 2013, http://dx.doi.org/10.1016/j.solmat.2013.04.017.
50. F. Fabregat-Santiago, J. Bisquert, G. Garcia-Belmonte, G. Boschloo, and A. Hagfeldt, *Sol. Energy Mater. Sol. Cells*, 2005, **87**, 117–131.
51. F. Fabregat-Santiago, G. Garcia-Belmonte, I. Mora-Seró, and J. Bisquert, *Phys. Chem. Chem. Phys.*, 2011, **13**, 9083–118.

